Redox Biology 70 (2024) 103067

Contents lists available at ScienceDirect

Redox Biology

journal homepage: www.elsevier.com/locate/redox

FTO ameliorates doxorubicin-induced cardiotoxicity by inhibiting ferroptosis via P53–P21/Nrf2 activation in a HuR-dependent m6A manner

Yunfan Yang [a,1], Jiajun Ren [a,1], Jifeng Zhang [b], Henghe Shi [a], Junnan Wang [a,**], Youyou Yan [a,*]

[a] Department of Cardiology, Second Hospital of Jilin University, Changchun, Jilin, 130041, China
[b] School of Pharmaceutical Sciences, Jilin University, No. 218 Xinmin Street, Changchun, 130041, China

ARTICLE INFO

Keywords:
Doxorubicin
Ferroptosis
FTO
P53
P21
HuR
m6A modification

ABSTRACT

Doxorubicin (DOX)-induced cardiotoxicity seriously limits its clinical applicability, and no therapeutic interventions are available. Ferroptosis, an iron-dependent regulated cell death characterised by lipid peroxidation, plays a pivotal role in DOX-induced cardiotoxicity. N6-methyladenosine (m6A) methylation is the most frequent type of RNA modification and involved in DOX-induced ferroptosis, however, its underlying mechanism remains unclear. P21 was recently found to inhibit ferroptosis by interacting with Nrf2 and is regulated in a P53-dependent or independent manner, such as through m6A modification. In the present study, we investigated the mechanism underlying m6A modification in DOX-induced ferroptosis by focusing on P21. Our results show that fat mass and obesity–associated protein (FTO) down-regulation was associated with DOX-induced cardiotoxicity. FTO over-expression significantly improved cardiac function and cell viability in DOX-treated mouse hearts and H9C2 cells. FTO over-expression significantly inhibited DOX-induced ferroptosis, and the Fer-1 inhibition of ferroptosis significantly reduced DOX-induced cardiotoxicity. P21 was significantly upregulated by FTO and activated Nrf2, playing a crucial role in the anti-ferroptotic effect. FTO upregulated P21/Nrf2 in a P53-dependent manner by mediating the demethylation of P53 or in a P53-independent manner by mediating P21/Nrf2 directly. Human antigen R (HuR) is crucial for FTO-mediated regulation of ferroptosis and P53–P21/Nrf2. Notably, we also found that P21 inhibition in turn inhibited HuR and P53 expression, while HuR inhibition further inhibited FTO expression. RNA immunoprecipitation assay showed that HuR binds to the transcripts of FTO and itself. Collectively, FTO inhibited DOX-induced ferroptosis via P21/Nrf2 activation by mediating the m6A demethylation of P53 or P21/Nrf2 in a HuR-dependent manner and constituted a positive feedback loop with HuR and P53–P21. Our findings provide novel insight into key functional mechanisms associated with DOX-induced cardiotoxicity and elucidate a possible therapeutic approach.

1. Introduction

Cardiac death caused by chemotherapy is a major burden for cancer survivors [1]. Doxorubicin (DOX) has been widely used for the treatment of various cancers since 1960, but DOX-induced cardiotoxicity is found in about 41 % of cancer patients [2,3]. Ferroptosis, an iron-dependent regulated cell death characterized by lipid peroxidation, is an important mechanism in DOX-mediated cardiotoxicity [3]. In DOX-induced cardiomyopathy, ferroptosis inhibitor ferrostatin-1 (Fer-1) more effectively reduced DOX-induced mortality than apoptosis, necroptosis, or autophagy inhibitors [4]. It was found that DOX induced mitochondria-dependent ferroptosis by inhibiting glutathione peroxidase 4 (GPX4) via regulation of the cystine-glutamate exchanger (xCT, also known as SLC7A11) and nuclear factor erythroid-2 related factor 2 (Nrf2) [5,6]. However, the molecular mechanism of ferroptosis in DOX-induced cardiotoxicity is still unclear.

N6-methyladenosine (m6A) methylation, the most frequent type of RNA modification, is regulated by m6A methyltransferase (writers) such as methyltransferase-like 3/14 (METTL3/METTL14), m6A demethylase (erasers) such as fat mass and obesity-associated protein (FTO), ALKB homolog 5 (ALKBH5), and methylation reading protein (readers) such as YTH domain-containing family proteins [7]. Recent studies have shown that m6A participates in various diseases, including cardiovascular

* Corresponding author.
** Corresponding author.
E-mail addresses: jdeywjn@163.com (J. Wang), yanuu@jlu.edu.cn (Y. Yan).
[1] The same contribution.

https://doi.org/10.1016/j.redox.2024.103067
Received 22 January 2024; Accepted 29 January 2024
Available online 2 February 2024

Abbreviations

DOX	doxorubicin
m6A	N6-methyladenosine
GPX4	glutathione peroxidase 4
xCT	cystine-glutamate exchanger
FTO	fat mass and obesity-associated protein
ALKBH5	ALKB homolog 5
Nrf2	nuclear factor erythroid 2-related factor 2
HuR	human antigen R
AAV9	adeno-associated virus 9
LVEDV	left ventricular end-diastolic volume
LVIDd	left ventricular internal diameter diastolic
LVESV	left ventricular end-systolic volume
LVIDs	left ventricular internal diameter systolic
LVEF	left ventricular ejection fraction
LVFS	left ventricular fractional shortening

diseases, by regulating ferroptosis [7–9]. MELLT3 accelerates sepsis-induced myocardial injury by regulating m6A-dependent ferroptosis [8]. Similarly, METTL14 promotes DOX-induced ferroptosis by catalysing m6A modification of the long non-coding RNA KCNQ1OT1 [10]. FTO was first reported as an m6A demethylase and its expression decreased with DOX treatment [11]. Another study showed that FTO repressed radiation-induced ferroptosis of nasopharyngeal carcinoma [12]. In contrast, FTO prevents thyroid cancer progression by promoting ferroptosis via xCT inhibition [13]. Therefore, the mechanism underlying m6A modification in DOX-induced ferroptosis requires further investigation.

P21 has been found to inhibit DOX-induced cardiotoxicity by reducing mitochondrial dysfunction of cardiomyocytes [14,15]. P21 has been found to interact with Nrf2 [16], which enhances the expression of many anti-ferroptosis proteins, such as xCT, GPX4, haeme oxygenase-1 (HO-1), and NAD(P)H quinone oxidoreductase 1 (NQO-1) [17]. P21 regulation occurs primarily in P53-dependent or independent manners [18,19]. However, P53 also promotes ferroptosis by inhibiting xCT transcription [19]. P21 has also been found to hinder ferroptosis progression in a P53-independent manner [14]. M6A modification mediated by METTL3 is involved in post-transcriptional regulation of P21 in mouse breast cancer models [20,21]. Similarly, FTO is associated with P21 up-regulation in IL-17A-induced endothelial cell senescence [22]. Moreover, ELAV-like RNA binding protein 1 (ELAVL1)/Human antigen R (HuR) is a well-established RNA stabiliser and RNA-binding protein that is viewed as an m6A reader and is involved in the regulation of m6A-containing mRNA stabilisation and target translation [23]. As an mRNA-binding protein, HuR regulates the stability of several mRNAs including P21 [24]. These findings indicate that the m6A modification of P21 may be involved in DOX-induced ferroptosis.

In this study, we aimed to determine the effect of m6A modification on DOX-induced cardiotoxicity and investigate its underlying mechanism by focusing on P21 and ferroptosis in vivo and in vitro.

2. Materials and methods

2.1. Animal experiments

All mouse studies were performed in the Animal Lab of Jilin University and approved by the Institutional Animal Care and Use Committee of Jilin University (2023227). C57BL/6J mice (5–6 weeks of age) were tail-vein injected with a viral titter of 10^{13} adeno-associated virus 9 (AAV9) carrying FTO. Three weeks later, mice were intraperitoneally injected with DOX (Selleck) (5 mg/kg) twice a week for 5 weeks to establish a mouse model of DOX-induced cardiotoxicity.

2.2. Echocardiography

Mice were weighed and anaesthetised using 1.5 % isoflurane inhalation. Chemical hair remover (Veet, Reckitt Benckise, Granollers, Spain) and gel (Quick Eco-Gel, Lessa, Barcelona, Spain) were applied to the chests of mice before probe placement. The left ventricular end-diastolic volume (LVEDV), internal diameter diastolic (LVIDd), end-systolic volume (LVESV), and internal diameter systolic (LVIDs) were measured using a Vevo 2100 image system (VisualSonics, Toronto, Canada). Fractional shortening (FS) (%) was calculated as 100x((LVIDd-LVIDs)/LVIDd), and the ejection fraction (EF) (%) was calculated as 100x((LVEDV-LVESV)/LVEDV).

2.3. Tissue Processing

The mice were sedated with 1.5 % isoflurane and euthanised via thoracotomy. Mouse heart tissues were removed, weighed, and flash-frozen in liquid nitrogen or fixed in 4 % paraformaldehyde for further analysis.

2.4. Hematoxylin and eosin (H&E) and Masson staining

Cardiac paraffin sections were dewaxed and hydrated. Then, the sections were staining with H&E and Masson's trichrome according to the manufacturer's instructions. The images were acquired using an Olympus microscope.

2.5. Cell transfection

Lentiviruses expressing sh-FTO (sh-FTO), empty vector (NC), and pcDNA3.1-FTO (FTO-OE) were purchased from GeneChem Co. Ltd. (Shanghai) and used to infect H9C2 cells. Transfected cells were selected using puromycin (5 μg/ml) for 7 days or more. In addition to the lentiviruses, siRNA targeting P21 (Genechem Co. Ltd) (25 μmol/L) was transfected into normal or FTO over-expressing H9C2 cells using lipofectamine 2000 according to the manufacturer's instructions (Invitrogen). The following sequences of P21 siRNA were used: sense, 5-CGGUGGAACUUUGACUUCG-3 and antisense, 5- CGAAGUCAAAGUUCCACCG-3.

2.6. Cell viability assay

A Cell Counting Kit-8 (CCK8, Invitrogen) was used to evaluate cell viability. Briefly, 2×10^4 normal or transfected H9C2 cells/well were seeded into 96-well plates and then treated with DOX alone or plus HuR inhibitor, KH-3 (Selleck) or Fer-1 (Selleck) for 24 h; then, 10 μl CCK8 reagent was added to each group and cultured for 2 h. Finally, the absorbance was measured at 450 nm by a microplate reader to evaluate cell viability.

2.7. Detection of intracellular Fe^{2+} level

FerroOrange (Abcam; ab83366) was used to test the intracellular Fe^{2+} levels under a fluorescence microscope (Olympus Corporation), according to the manufacturer's protocol.

2.8. Measurement of intracellular reactive oxygen species (ROS)

ROS production was measured using dihydroethidium (DHE, S0063; Beyotime) in the H9C2 cells according to the manufacturer's instructions. Briefly, 2.5 μM DHE was added and incubated in H9C2 cells for 30 min at 37 °C in a dark environment, and the fluorescence was measured to evaluate ROS production using fluorescence microscopy (Olympus Corporation).

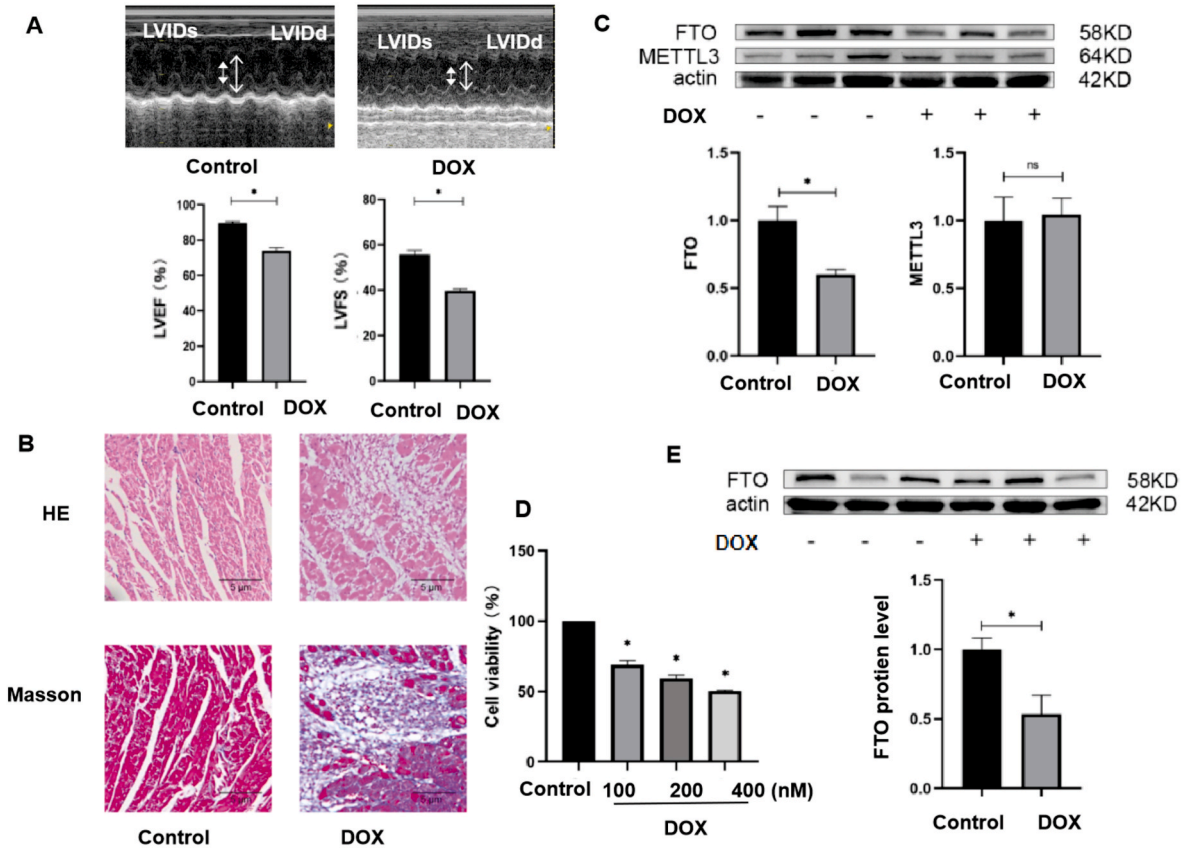

Fig. 1. FTO and METTL3 expression in DOX-treated mouse hearts or H9C2 cells. (A) Preserved left ventricular ejection fraction (EF) and fractional shortening (FS) in DOX-treated mice as evidenced by echocardiography (*, $P < 0.05$, 4 mice/group, respectively). (B) Representative images of hematoxylin-eosin staining (H&E) and Masson staining of the myocardial tissues in DOX-treated mice (scale bar = 5 μm). (C) The expression of FTO and METTL3 in the hearts of DOX-treated mice were detected by Western blotting (*, $P < 0.05$, 3 mice/group). (D) The effect of different doses of DOX on cell viability. CCK-8 assay was performed to evaluate viability of H9C2 cells treated with DOX at 0–400 nM for 24 h (*, $P < 0.05$, $n = 3$). (E) The protein level of FTO in H9C2 cells treated PBS (control) and 200 nM DOX (*, $P < 0.05$, $n = 3$).

2.9. Transmission Electron microscopy

Normal and transfected H9C2 cells were treated with DOX (200 nM) for 24 h and then collected and placed in 2.5 % glutaraldehyde phosphate overnight at 4 °C, then fixed in 2 % buffered osmium tetraoxide, and finally embedded in Epon812 (Merck), followed by dehydration. Ultrathin sections (60 nm in thickness) were cut and stained with uranyl acetate and lead citrate were used for staining. Finally, a TEM microscope was used for image checking (Ftmicro, Japan).

2.10. RNA Isolation and qPCR

Total RNA was isolated using TRIzol Reagent (Transgen). RNA (500 ng) was synthesised into cDNA, and the related mRNA levels were detected using EasyScript All-in-One First-Strand cDNA Synthesis SuperMix and TransStart Green qPCR SuperMix (Transgen). The FTO primers were as follows: forward, GCTGTGGAAGAAGATGGAGAGTGTG; reverse, AGTGGGATCAGGACGGCAGAC.

2.11. Protein Isolation and western blotting

Total protein was isolated from crushed tissues in RIPA buffer or from H9C2 or AC16 cells in buffer and protease inhibitor (Beyotime). Then, 25 μg of protein extract per lane was separated on a 10 % polyacrylamide gel and transferred to a nitrocellulose membrane. Blocking was performed for 1 h at room temperature using 5 % BSA albumin in 0.1 % Tween 20 and tris-buffered saline (T-TBS). Primary antibodies against FTO, METTL3, HuR, P53, P21, Nrf2, GPX4, FTH1, HO-1, xCT, TFR, ACSL4, and β-actin (Abcam, ABclonal, Proteintech), were incubated overnight at 4 °C, and secondary antibodies were incubated for 1–2 h at room temperature in T-TBS. Images were captured and analysed using a ChemiDoc Imaging System and ImageLab software (Bio-Rad).

2.12. M6A quantification assay

M6A quantification assay was performed using the m6A RNA Methylation Quantification Kit (EpiQuik), following the manufacturer's instructions. Briefly, total RNA was extracted with TRIzol Reagent (Transgen), 200 ng of RNA sample and 2 μl of positive and negative control were added to the wells, and detection was performed at 450 nm using a microplate reader. The percentage of m6A in total RNA was calculated as follows:

$$([(\text{Sample OD} - \text{NC OD}) \div S] \div [(\text{PC OD} - \text{NC OD}) \div P]) \times 100\ \%$$

Where S: input sample RNA; P: input Positive Control.

2.13. RNA immunoprecipitation (RIP) assay

The RIP assay was performed on H9C2 cells using the Magna RIP Kit (GENESEED), following the manufacturer's instructions. Briefly, more than 2×10^7 H9C2 cells were lysed and incubated with magnetic beads pre-coated with 5 mg normal antibodies against HuR (ABclonal), or IgG negative control antibodies (ABclonal) were incubated with sufficient cell lysates (per sample) at 4 °C overnight. Proteinase K was added to digest the proteins in the immunoprecipitated RNA-protein complex,

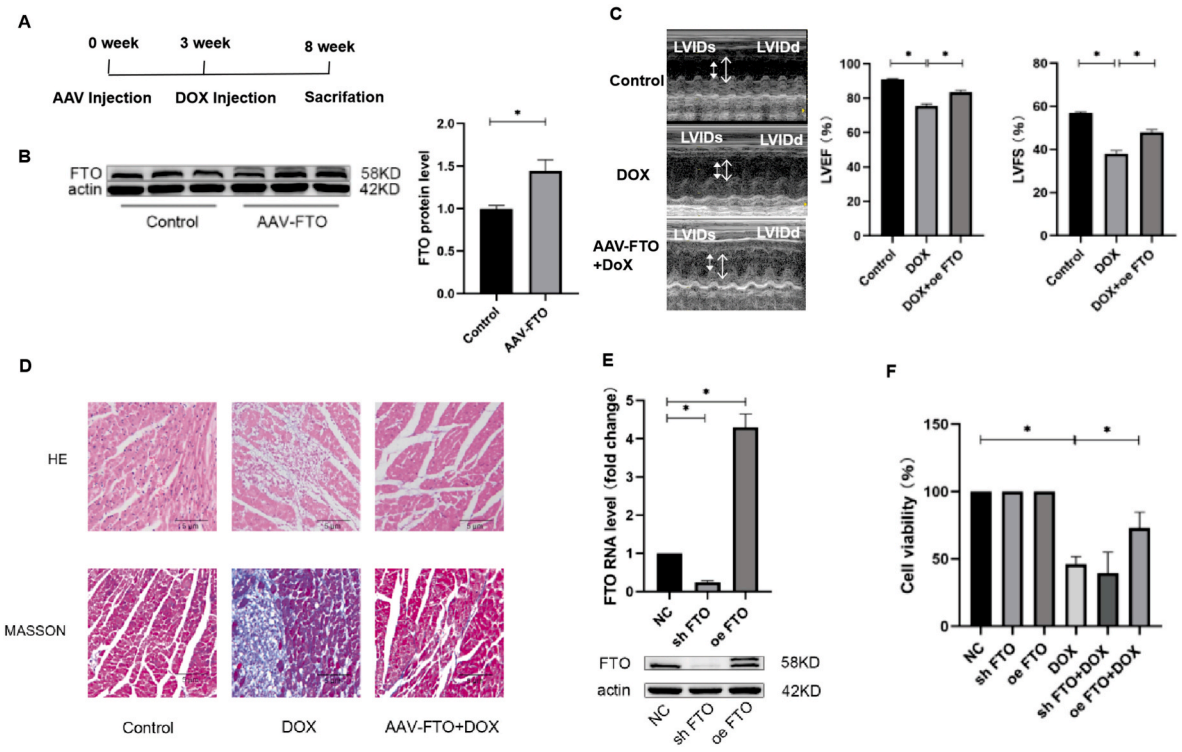

Fig. 2. Effect of FTO on DOX-induced cardiotoxicity in mice and H9C2 cells. (A) The schedule of adeno-associated virus 9 (AAV9)-FTO injection and DOX administration in mice. (B) Western blotting was used to confirm the expression of FTO in the hearts of mice injected with the AAV9-FTO before the DOX administration (*, $P < 0.05$, 3 mice/group). (C) The effect of FTO on cardiac function in DOX-treated mice. Mice were injected with AAV9-FTO and then treated with DOX, and preserved left ventricular ejection fraction (EF) and fractional shortening (FS) were assayed by echocardiography (*, $P < 0.05$, 4 mice/group). (D) Representative images of hematoxylin-eosin staining (H&E) and Masson's trichrome staining of the myocardial tissues (scale bar = 5 μm). (E) FTO-overexpressing (oe FTO) and-knockdown (sh FTO) H9C2 cell lines were constructed and confirmed at the mRNA and protein levels. (F) Effect of FTO on the viability of H9C2 cells treated with DOX. CCK8 assay was performed in normal or FTO-transfected H9C2 cells treated with PBS or 200 nM DOX for 24 h (*, $P < 0.05$, $n = 3$).

followed by TRIzol extraction of the precipitated RNAs. RNAs of interest were detected by RT-qPCR and normalised to the input (fold change was calculated for comparison). The following P53 primers were used: forward CAGCACAGGAACCTGGAACT, reverse GAGAAGGGACGGAAGATGAC. The following P21 primer was used for HuR-RIP: forward GGTGATGTCCGACCTGTTCC, reverse ACGCTCCCAGACGTAGTTGC. The following Nrf2 primer was used: forward TGACTCTGACTCCGGCATTT, reverse CCCCAGAAGAATGTGTTGGC.

2.14. M6A RNA immunoprecipitation assay (MeRIP)

Total RNAs of FTO-overexpressing and negative control H9C2 cells treated with DOX was isolated using TRIzol Reagent and then purified using the mRNA Purification Kit (BersinBio). The purified mRNA was fragmented into approximately 300 nt fragments using ZnCl2 on an ice-water mixture for 10s. Next, one-tenth volume of fragmented RNA was saved as "10 % input", and the rest of the fragments were incubated with 10 μg anti-m6A antibody or anti-mouse IgG antibody which linked to Magna ChIP Protein A/G Magnetic Beads. The extracted RNA was analysed using qPCR for P21 and Nrf2 and normalised to the input. The m6A sites of P53, P21 and Nrf2 were predicted using the SRAMP software (http://www.cuilab.cn/sramp). The specific primers for P53, P21, and Nrf2 for the Me-RIP assay were as follows P53: forward, CTCACACTGGCTAAAGTTCTGA; reverse, CGACTGTGAATCCTCCATGAC. P21: forward, CTGTGTTTCTGATCCTGGCG; reverse, GACCCCGAAGTCCTACTCAG. Nrf2: forward, TGACTCTGACTCCGGCATTT; reverse, CCCCAGAAGAATGTGTTGGC.

2.15. RNA stability assay

To determine effect of FTO on the stability of P53, P21 and Nrf2, an actinomycin D assay was performed in FTO over-expressing or normal H9C2 cells treated with 5 μg/ml actinomycin D (Sigma, St. Louis, MO, USA) at 0 h, 0.5h, 1h, 2h, and 4h. The mRNA expression of P53, P21 and Nrf2 was measured by RT−qPCR, the primers of P53, P21 and Nrf2 as indicated in RNA Immunoprecipitation (RIP) Assay.

2.16. Statistical analysis

All data are presented as means ± SE and were analysed using Student's t-test in GraphPad Prism (v. 9.1.0). The results were considered statistically significant at $p < 0.05$.

3. Results

3.1. Down-regulation of FTO in DOX-induced cardiotoxicity in vivo and vitro

To investigate whether m6A modification is involved in DOX-induced cardiotoxicity, we first evaluated the cardiac function and levels of METTL3 and FTO in the hearts of mice treated with DOX (5 mg/kg, twice per week for 5 weeks). Left ventricular ejection fraction (LVEF), an indicator of the percentage of blood volume pumping capacity, and left ventricular fractional shortening (LVFS), an indicator of the change in left ventricular diameter during systolic contraction, were assessed using echocardiography to evaluate cardiac function. As shown in Fig. 1A, both LVEF and LVFS were significantly reduced in DOX-treated mice, indicating that DOX significantly reduced cardiac

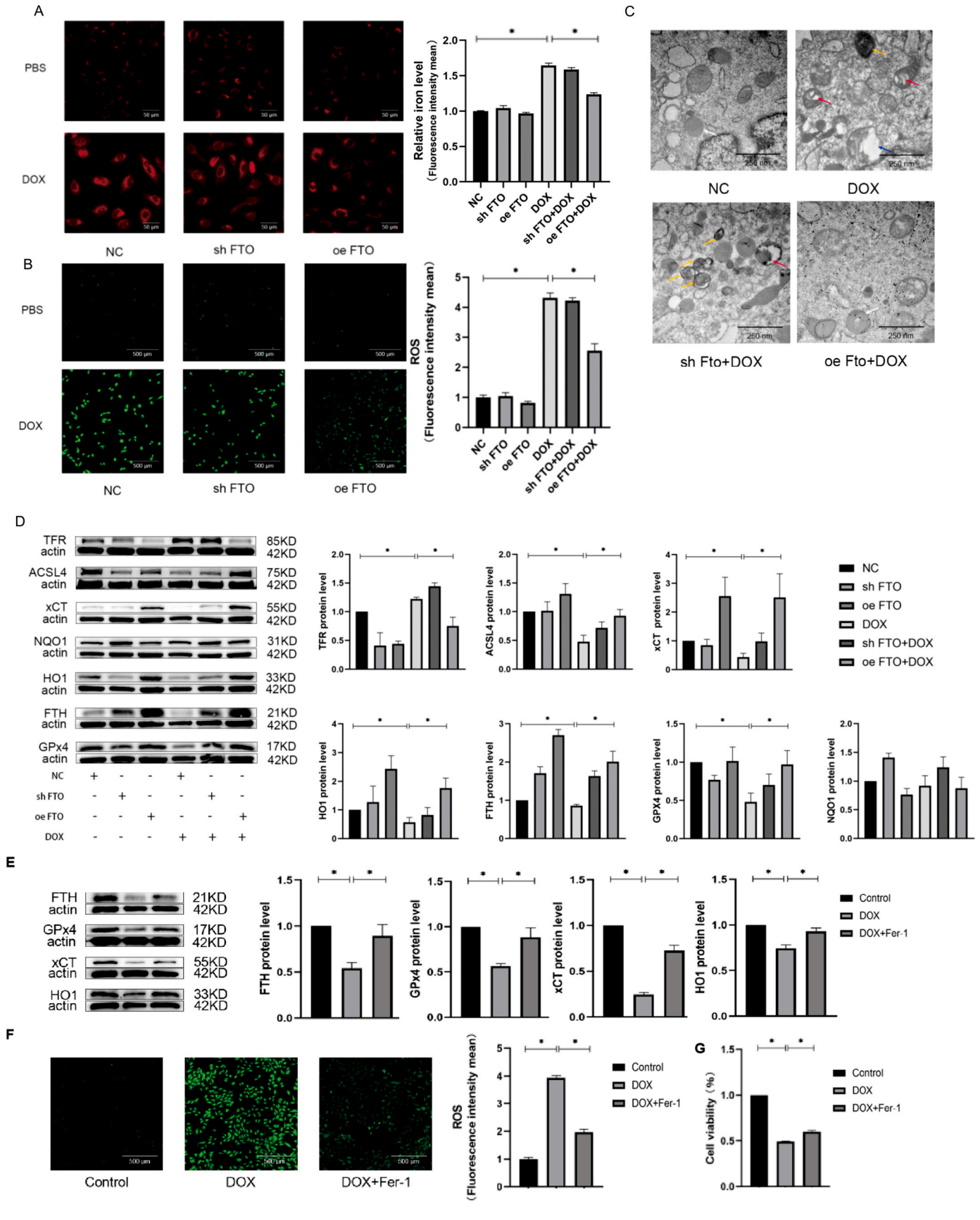

(caption on next page)

Fig. 3. Effect of FTO on DOX-induced ferroptosis in H9C2 cells (A) Intracellular Fe^{2+} level in the normal and FTO transfected H9C2 cells treated with or without DOX, as evidenced by FerroOrange staining (*, $P < 0.05$, scale bar = 50 μm). (B) Intracellular reactive oxygen species (ROS) level in the normal and FTO transfected H9C2 cells treated with PBS or DOX, as evidenced by dihydroethidium (DHE) staining (*, $P < 0.05$, scale bar = 500 μm). (C) Representative images of mitochondrial morphology in the normal and FTO transfected H9C2 cells treated with DOX. The white, yellow, blue and red arrow indicate normal mitochondrial morphology, increase of mitochondrial membrane density, mitochondrial membrane rupture, and the decrease or disappearance of mitochondrial cristae, respectively (scale bar = 250 μm, respectively). (D) The effect of FTO on the ferroptosis-related proteins in DOX-treated H9C2 cells. The expression of TFR, ACSL4, xCT, HO-1, FTH, GPX4, and NQO-1 in DOX-treated normal and FTO over-expressing H9C2 cells were assayed by Western blotting (*, $P < 0.05$, n = 3). (E) The effect of Fer-1 on the ferroptosis-related proteins in DOX-treated H9C2 cells. The expression of xCT, HO-1, FTH, and GPX4 in H9C2 cells treated with DOX alone or plus Fer-1 (*, $P < 0.05$, n = 3). (F) ROS level in H9C2 cells treated with DOX alone or plus Fer-1 (*, $P < 0.05$, scale bar = 500 μm). (G) The effect of Fer-1 on viability of H9C2 cells treated with DOX. CCK8 assay was performed in H9C2 cells treated with 200 nM DOX or plus Fer-1 (10 μM) for 24 h (*, $P < 0.05$, n = 3).

function. H&E and Masson staining showed that DOX significantly promoted structural abnormalities in the heart, including increased myofibre cross-sectional area and heart fibrosis (Fig. 1B). Western blotting showed that the FTO protein was significantly down-regulated in the hearts of DOX-treated mice, whereas the change in METLL3 was not significant between the DOX and control groups (Fig. 1C).

Next, we measured the FTO protein level in DOX-treated H9C2 cells. To determine the optimal concentration of DOX in H9C2 cells, we used the CCK8 to detect the activity of H9C2 cells under different doses of DOX (100, 200, and 400 nM). As shown in Fig. 1D, the viability of H9C2 cells significantly decreased in a dose-dependent manner after treatment with DOX for 24 h. The IC50 value of DOX was 200 nM, the dosage was optimised for subsequent experiments. We also tested the effect of DOX on FTO protein levels in H9C2 cells and found that FTO protein level significantly decreased in DOX-treated H9C2 cells (Fig. 1E).

3.2. FTO ameliorates DOX-induced cardiotoxicity in mice and H9C2 cells

To evaluate the role of FTO on DOX-induced cardiotoxicity, mice were tail vein-injected with viral titter of 10^{13} AAV9-FTO (300 μl) 3 weeks before being subjected to DOX injection, mice in control group were injected with PBS (Fig. 2A). We first confirmed that FTO was effectively over-expressed in the hearts of mice injected with AAV9-FTO before DOX administration (Fig. 2B). LVEF and FS decreased and cardiac fibrosis increased in DOX-treated mice, which was improved by AAV9-FTO injection (Fig. 2C and D). To further assess the protective effect of FTO against DOX-induced cardiotoxicity in vitro, FTO-overexpressing and-knockdown H9C2 cell lines were constructed and confirmed at the mRNA and protein levels (Fig. 2E). Next, the CCK8 assay was performed in normal or FTO-transfected H9C2 cells treated with or without 200 nM DOX for 24 h. The results showed that DOX significantly decreased the viability of H9C2 cells; this effect was accelerated by FTO knockdown and inhibited by FTO overexpression (Fig. 2F). These results suggested that FTO inhibited DOX-induced cardiotoxicity in mice and H9C2 cells.

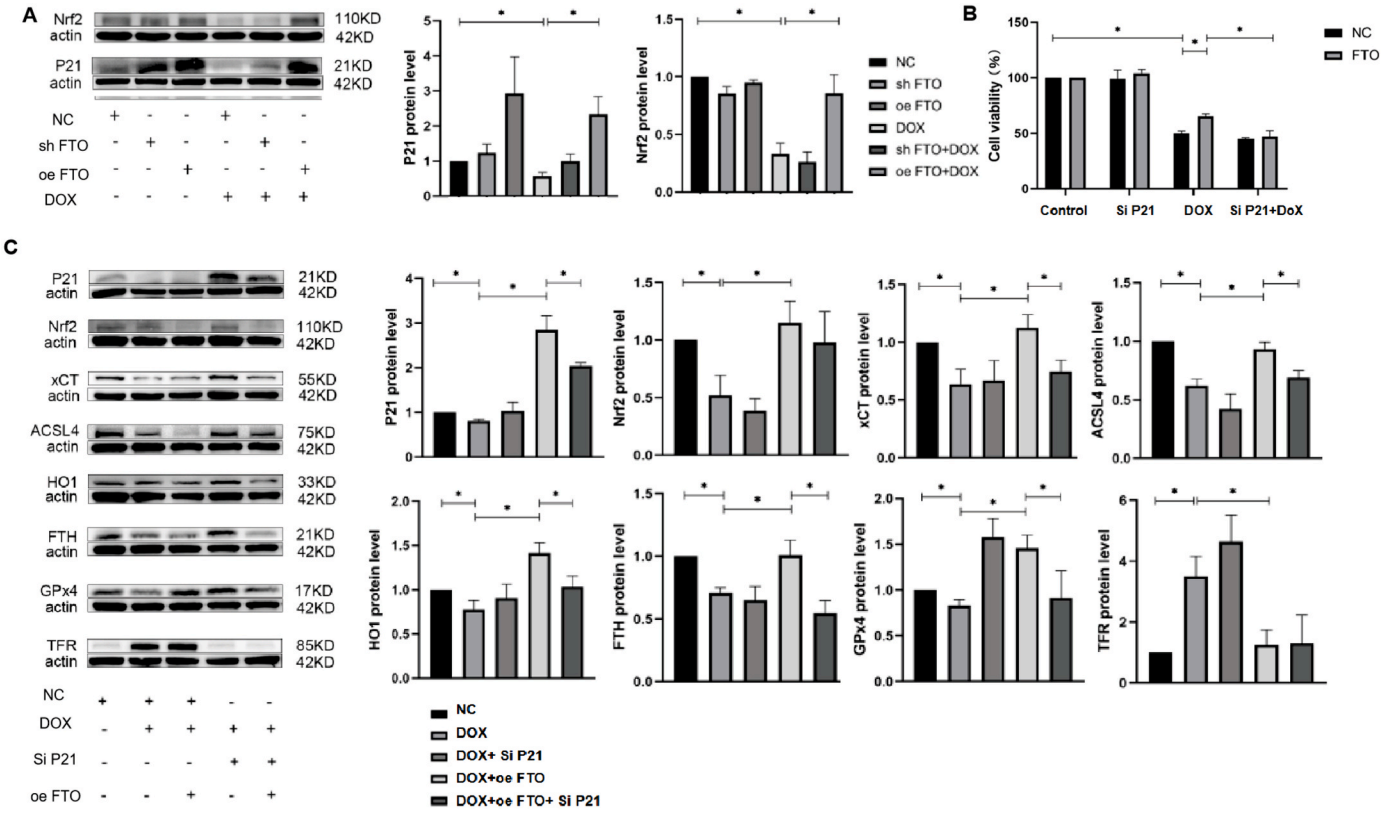

Fig. 4. The role of P21 in FTO-mediated regulation of Nrf2 and ferroptosis (A) Expression of P21 and Nrf2 in the normal and FTO-transferred H9C2 cells treated with DOX or PBS. (B) The effect of P21 in the regulation of FTO in viability of DOX-treated H9C2 cells. CCK8 assay was performed in normal and FTO over-expressing H9C2 cells transfected with siRNA-P21 and treated with PBS or 200 nM DOX for 24 h (*, $P < 0.05$, n = 3). (C) The effect of P21 on the regulation of FTO in ferroptosis-related proteins and Nrf2 in DOX-treated H9C2 cells. Normal and FTO over-expressing H9C2 cells were transfected with siRNA-P21 and then treated with 200 nM DOX for 24h.Western blotting analysis of P21, xCT, ACST4, HO-1, FTH, GPX4, TFR, and Nrf2 expression, which were standardized to those of β-actin (*, $P < 0.05$, n = 3).

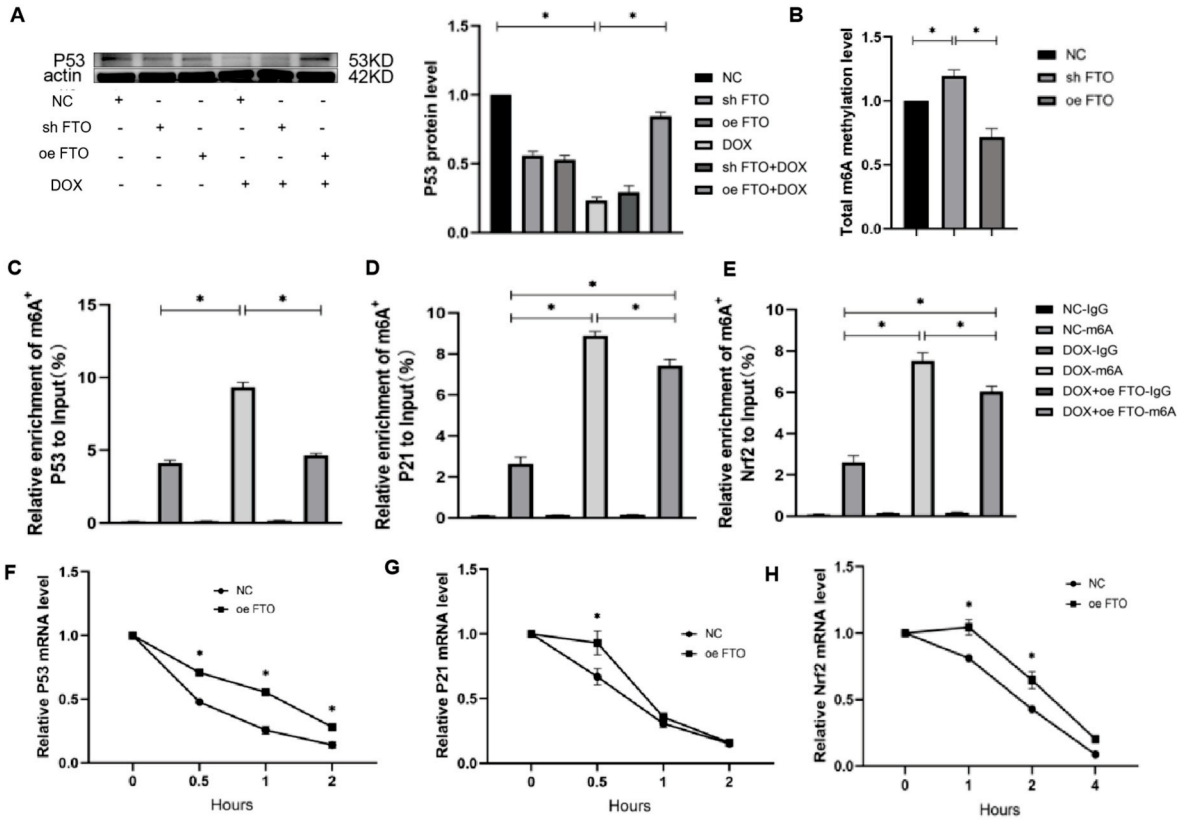

Fig. 5. m6A demethylation of P53, P21 and Nrf2 by FTO (A) Effect of FTO on P53 expression in DOX-treated H9C2 cells. (B) The total RNA N6 methyladenosine (m6A) level in the DOX-treated normal and FTO over-expressing H9C2 cells. (C–E) m6A modification of P53, P21 and Nrf2 by FTO in the DOX-treated H9C2 cells. Normal or FTO over-expressing H9C2 cells were incubated in a medium with DOX at 200 nM for 24 h, and the m6A percentage of P53 (C), P21(D) and Nrf2 (E) mRNA was calculated by MeRIP-qPCR. (F–H) The effect of FTO on stability of P53, P21 and Nrf2 mRNA. Degradation curves of P53 (F), P21 (G) and Nrf2 (H) mRNA in normal and FTO over-expressing H9C2 cells treated with actinomycin D were generated by qRT-PCR assay at the indicated times (*, $P < 0.05$, $n = 3$).

3.3. FTO protects against DOX-induced cardiotoxicity by inhibiting ferroptosis

We investigated whether FTO protects against DOX-induced cardiotoxicity by regulating ferroptosis. We first investigated the effects of DOX and FTO on intracellular Fe^{2+} and ROS levels in H9C2 cells. The fluorescence results showed that DOX significantly increased Fe^{2+} and ROS production in H9C2 cells, which was significantly enhanced by FTO knockdown and inhibited by FTO overexpression (Fig. 3A and B). Moreover, cell morphology analysis showed that the mitochondria in DOX-treated H9C2 cells were smaller, accompanied by increased membrane density and decreased cristae (Fig. 3C). The change in mitochondria was smaller in FTO-overexpressing H9C2 cells treated with DOX. Next, we assayed the effects of FTO on ferroptosis-related proteins. As shown in Fig. 3D, DOX significantly inhibited the expression of anti-ferroptotic proteins, including GPX4, FTH1, HO-1, xCT, and NQO-1, and enhanced the expression of the pro-ferroptotic protein TFR in H9C2 cells. Notably, the level of ACSL4, a pro-ferroptotic protein, was decreased after DOX treatment. In contrast, FTO overexpression significantly inhibited the expression of GPX4, FTH1, HO-1, xCT, and TFR, but significantly enhanced the expression of ACSL4 in H9C2 cells. However, there was no significant difference in NQO-1 expression between normal and FTO overexpressing H9C2 cells under DOX treatment. This suggests that FTO inhibits DOX-induced ferroptosis.

We also investigated the role of ferroptosis in DOX-induced cardiotoxicity by adding ferroptosis inhibitor Fer-1 to DOX treatment. The results showed that Fer-1 inhibited DOX-induced decrease in anti-ferroptosis proteins, including GPX4, FTH1, HO-1, and xCT, in H9C2 cells (Fig. 3E). Furthermore, we found that Fer-1 significantly reduced ROS production and limited the DOX-induced reduction in H9C2 cell viability (Fig. 3F and G). These results suggest that ferroptosis inhibition is involved in the protective effects of FTO against DOX-induced cardiotoxicity.

3.4. P21 is essential for FTO- mediated regulation of Nrf2 and ferroptosis

P21 was reported to inhibit ferroptosis by interacting with Nrf2, which enhances the expression of many anti-ferroptosis proteins [16]. To investigate whether P21 participates in the antiferroptotic effect of FTO through the Nrf2 signalling pathway, we first evaluated the effect of FTO and DOX on P21 and Nrf2 expression in H9C2 cells. The results showed that DOX significantly decreased the expression of P21 and Nrf2, whereas the DOX-induced decrease in P21 and Nrf2 was significantly inhibited by FTO overexpression (Fig. 4A). We further assayed the role of P21 in the FTO-mediated regulation of Nrf2 using siRNA-P21, P21 protein level was confirmed by western blotting (Fig. 4C). The results showed that FTO overexpression significantly inhibited the DOX-induced decrease in Nrf2, but siRNA-P21 reduced the regulation of FTO on Nrf2, and there was no significant difference in Nrf2 between the DOX group and the DOX plus FTO and siRNA-P21 groups. This indicates that P21 is involved in the regulation of Nrf2 by FTO.

Next, we confirmed the role of P21 in the anti-ferroptotic effect of FTO and found that the inhibition of P21 significantly accelerated the DOX-induced decrease in cell variability and reduced the improvement of FTO overexpression in cell variability (Fig. 4B). Moreover, P21 inhibition blocked the regulation of FTO in ferroptosis-related proteins, including GPX4, FTH1, HO-1, xCT, and ACSL4. However, no significant difference was observed in the TFR between FTO and FTO plus siRNA-P21 in DOX-treated H9C2 cells (Fig. 4C). This suggests that P21 is involved in ferroptosis regulation by FTO.

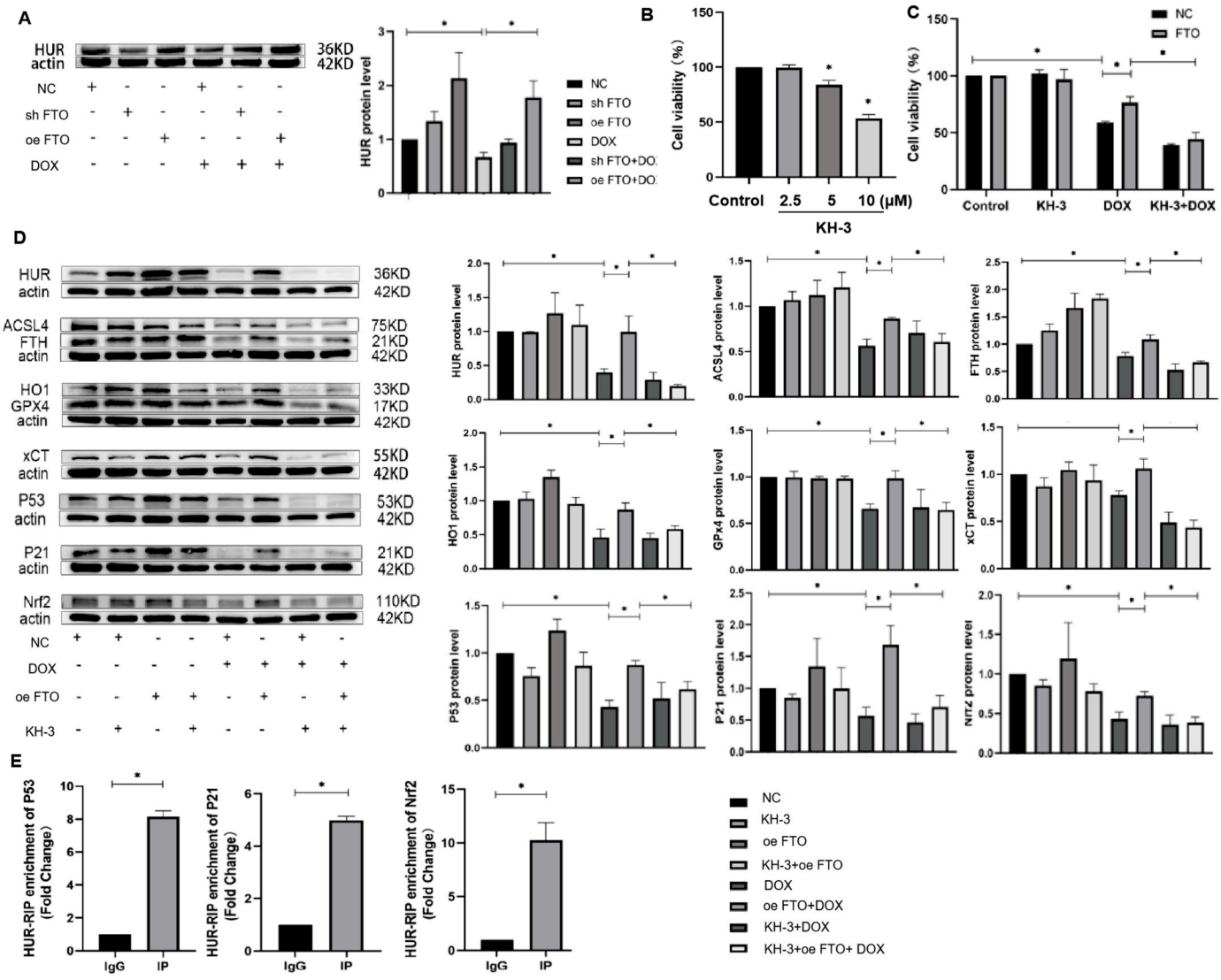

Fig. 6. The role of HuR on FTO-mediated regulation of ferroptosis and P53–P21/Nrf2 (A) Western blot analysis of HuR expression in DOX-treated normal or FTO transfected H9C2 cells. (B) CCK8 assay was performed in H9C2 cells treated with different doses of KH-3. (C) CCK8 assay was performed in normal or FTO-transfected H9C2 cells treated with DOX alone or plus 2.5 μM KH-3. (D) The role of HuR in FTO-mediated regulation of ferroptosis-related proteins and P53/P21/Nrf2. Normal and FTO over-expressing H9C2 cells were treated with 200 nM DOX and/or 2.5 μM KH-3, and HuR, the ferroptosis-related proteins including ACSL4, xCT, HO-1, FTH, and GPX4, and P53/P21/Nrf2 were assayed by western blotting (*, $P < 0.05$, $n = 3$). (E) The interactions of HuR with P53, P21 and Nrf2 were verified in HuR-RIP by qPCR (*, $P < 0.05$, $n = 3$).

3.5. FTO regulates P53 and P21/Nrf2 by mediating m6A demethylation

P21 is typically regulated in P53-dependent or independent manners. To explore the mechanism underlying P21/Nrf2 regulation by FTO, we first assayed the regulation of FTO on P53, which is up-stream of P21. As shown in Fig. 5A, DOX significantly decreased the expression of P53, while FTO over-expression significantly reduced the DOX-induced decrease in P53, indicating that FTO up-regulated P21/Nrf2 by activating P53. M6A quantification assay showed that FTO significantly reduced the increased m6A levels induced by DOX in H9C2 cells (Fig. 5B), indicating that FTO activated P53 by mediating m6A demethylation. The MeRIP results showed that DOX significantly enhanced m6A levels in P53 mRNA, which was significantly inhibited by FTO over-expression in H9C2 cells (Fig. 5C). Furthermore, FTO over-expression increased the half-life of P53 mRNA in H9C2 cells treated with actinomycin D (Fig. 5F).

In addition to a P53-dependent manner, P21 and Nrf2 have also been reported to be regulated by FTO-mediated m6A methylation. The MeRIP results also showed that DOX significantly enhanced the m6A levels of P21 and Nrf2 mRNA, which were significantly inhibited by FTO over-expression in H9C2 cells (Fig. 5D and E). Consistently, we found that FTO overexpression enhanced the half-life of P21 and Nrf2 mRNA upon actinomycin D treatment (Fig. 5G and H). This evidence suggests FTO activates P21/Nrf2 in a P53-dependent or-independent manner by mediating m6A demethylation of P53 or P21/Nrf2.

3.6. HuR is crucial for FTO-mediated regulation of ferroptosis and P53–P21/Nrf2

To gain further insight into the mechanism underlying the m6A modification of P53, P21 and Nrf2 by FTO, we tested the expression of HuR, which has been reported to enhance the stability of mRNA and assist in m6A modification [23,24]. Our data showed that HuR expression was significantly decreased by DOX but increased by FTO over-expression (Fig. 6A). To investigate the role of HuR in the protective effect of FTO against DOX-induced cardiotoxicity, a HuR inhibitor, KH-3, was added, as it has been reported to mimic genetic HuR knockout by CRISPR [25]. We first determined the optimal concentration of KH-3

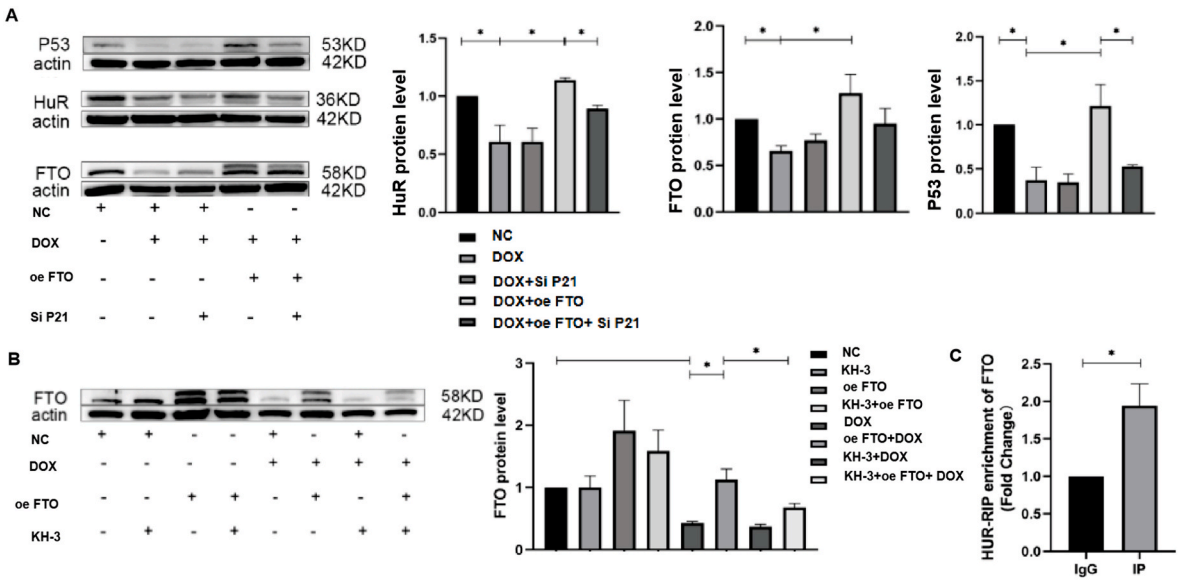

Fig. 7. Interact regulations of P53–P21, HuR, and FTO (A) Effect of P21 on the expression of P53, HuR and FTO. Western blotting analysis of P53, HuR and FTO in normal or FTO over-expressing H9C2 cells were transfected with siRNA-P21 and treated with PBS or 200 nM DOX for 24h (*, $P < 0.05$, $n = 3$). (B) The effect of HuR on the expression of FTO in DOX-treated H9C2 cells. Western blotting analysis of FTO in normal or FTO over-expressing H9C2 cells were treated with DOX and/or KH-3. (*, $P < 0.05$, $n = 3$). (C) The interaction of HuR with FTO was verified in HuR- RIP by qPCR (*, $P < 0.05$, $n = 3$).

and the CCK8 assay was performed in H9C2 cells. The results showed that there was no effect of KH-3 at 2.5 μM on cell viability, while KH-3 at 5 or 10 μM significantly inhibited the cell viability; thus, 2.5 μM KH-3 was selected for subsequent experiments (Fig. 6B). We further found that HuR inhibition using KH-3 significantly accelerated the DOX-induced decrease in cell viability and significantly inhibited the improvement of FTO overexpression in cell viability (Fig. 6C). Moreover, we tested the effect of HuR on the regulation of FTO in ferroptosis in DOX-treated H9C2 cells. The results showed that inhibition of HuR by KH-3 blocked the regulations of FTO in ferroptosis-related proteins xCT, GPX4, FTH1, HO-1, and ACSL4 in DOX-treated H9C2 cells (Fig. 6D).

We next investigated the role of HuR in the FTO-mediated regulation of P53–P21/Nrf2. Our data showed that KH-3 blocked the up-regulation of P53, P21, and Nrf2 by FTO in DOX-treated H9C2 cells. Significant enrichment of P53, P21, and Nrf2 transcripts were found in HuR-RIP, suggesting that HuR could bind to P53, P21, and Nrf2 transcripts to enhance their stability (Fig. 6E).

3.7. Interact regulations of P53–P21, HuR, and FTO

Our data showed that the inhibition of P21 in turn, decreased the expression of HuR and P53 (Fig. 7A), indicating that P21 also positively upregulated the expression of HuR and P53. Moreover, inhibition of HuR using KH-3 significantly reduced the expression of FTO and HuR in H9C2 cells (Fig. 7B), suggesting HuR also up-regulated the expression of FTO. Furthermore, a HuR-RIP assay was performed to test the binding of HuR and FTO mRNA and showed significant enrichment of FTO and HuR transcripts in HuR-RIP (Fig. 7C), indicating that HuR could regulate FTO and itself. This suggests that there is a positive feedback loop for P53–P21, HuR, and FTO.

4. Discussion

In this study, we found that FTO was significantly decreased in DOX-treated mice and H9C2 cells, and FTO mediated protective effect against DOX-induced cardiotoxicity by inhibiting ferroptosis via P21/Nrf2 activation. The activation of P21/Nrf2 by FTO was associated with m6A demethylation of P53, P21/Nrf2 mRNA, indicating that FTO activates P21/Nrf2 in both a P53-dependent and-independent manner. Moreover, HuR is crucial for the regulation of FTO in ferroptosis and P53, P21/Nrf2. Furthermore, our data also showed that inhibition of P21 in turn inhibited the HuR and P53, and inhibition of HuR also inhibited the FTO and itself, indicating that there was a positive feedback loop of FTO/HuR/P53–P21.

Our and other studies showed that ferroptosis occurred in DOX-induced cardiotoxicity with the increase of m6A levels [3]. It is favored that m6A modifications are involved in the regulations of ferroptosis and that the key regulators of ferroptosis also exhibit aberrant m6A levels under different pathological conditions [26]. FTO represses radiation-induced ferroptosis of nasopharyngeal carcinoma [27]. Consistently, our data showed that FTO expression was decreased by DOX and FTO overexpression inhibited DOX-induced ferroptosis by inhibiting Fe^{2+} and ROS production. In addition, we found that the ferroptosis inhibitor Fer-1 significantly inhibited ROS production and reduced the doxorubicin-induced cardiotoxicity. Consistently, the ferroptosis inhibitor Fer-1 more effectively reduced DOX-induced mortality than apoptosis, necroptosis, or autophagy inhibitors, suggesting that ferroptosis is more important than apoptosis, necroptosis, or autophagy in doxorubicin-induced cardiomyopathy [4]. This suggests that FTO protects against DOX-induced cardiotoxicity mainly through the inhibition of ferroptosis. FTO was also found to promote ferroptosis in thyroid cancer by inhibiting xCT via the regulation of m6A methylation [28]. Similarly, ALKBH5 also belongs to ALKB and is found to promote ferroptosis in thyroid cancer, but inhibit ferroptosis in glioblastoma [29,30]. In this study, FTO promoted the expression of antiferroptosis proteins, including GPX4, FTH1, HO-1, and xCT, and inhibited the expression of the proferroptosis protein TFR. However, we also found that ACSL4, a proferroptosis protein, was decreased by DOX but increased by FTO overexpression. Therefore, the contrasting effect of FTO on the pro-ferroptosis protein TFR/ACSL4 might be attributed to the dual role of FTO in ferroptosis reported in different studies.

Recently, P21 was found to inhibit ferroptosis and exert protective effects against DOX-induced cardiotoxicity [14]. For example, P21 was decreased following DOX treatment and is associated with exacerbated mitochondrial dysfunction and cardiomyocyte apoptosis [31]. P21 up-regulation resulted in G2/M phase cell cycle arrest and prevented DOX-induced H9C2 cell death [32]. Our data showed that FTO reduced the DOX-induced decrease in P21, and the inhibition of P21 reduced the

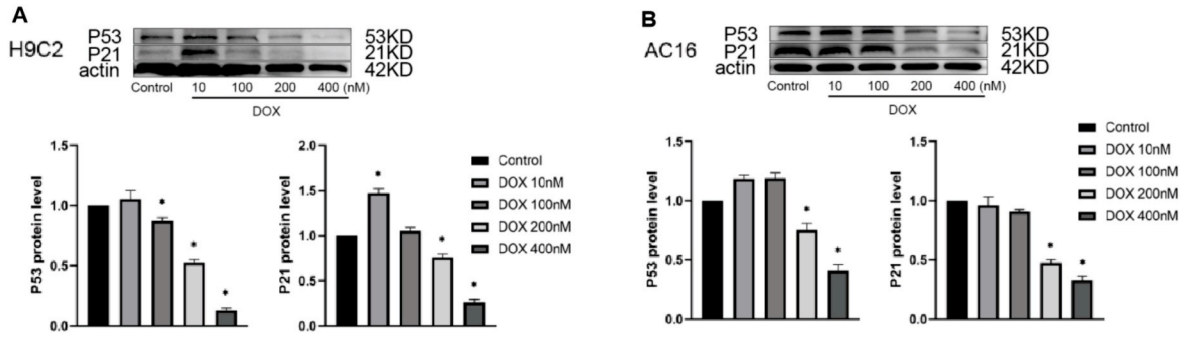

Fig. 8. The effect of different doses of DOX on P53 and P21 protein in H9C2 or AC16 cells. (A) The effect of different doses of DOX on expression of P53 and P21 in H9C2 cells.(B) The effect of different doses of DOX on expression of P53 and P21 in AC16 cells. Western blotting analysis of P53 and P21 in H9C2 or AC16 cells treated with DOX at 0, 10, 100, 200 and 400 nM for 24 h (*, $P < 0.05$, $n = 3$).

anti-ferroptosis effect of FTO. A P53-independent inhibitor of P21, UC2288 was found to increase radiation-induced oxidative stress and lipid peroxidation [33]. P21 has been reported to activate Nrf2, which, in turn up-regulated P21 [16,34]. Nrf2 has been reported to promote the expression of many anti-ferroptosis proteins, such as xCT, GPX4, HO-1, and FTH1 [17]. Consistently, we found that FTO overexpression significantly reduced DOX-induced decrease of Nrf2. However, siRNA-P21 reduced the regulation of FTO on Nrf2, and there was no significant difference in Nrf2 between the DOX group and the DOX plus FTO and siRNA-P21 group, indicating P21 is crucial for the activation of Nrf2 by FTO.

P21 is regulated in a P53-dependent or independent manner. Similar to P21, P53 was significantly decreased by DOX and upregulated by FTO overexpression in this study, indicating that FTO up-regulated P21 by activating P53. A previous study found that P53 activation is closely related to mRNA demethylation in DOX-treated hepatocellular carcinoma [35]. Similarly, we found that FTO up-regulated P53 by mediating its mRNA demethylation, indicating that FTO up-regulated P21 in a P53 dependent manner. In addition, MAPK, selenium-binding protein 1, and iNOS induce P21 expression in a P53-independent manner [36,37]. Moreover, P21 expression was regulated by m6A methylation. For example, METTL3 and METTL16 inhibited the expression of P21 by mediating m6A modification in breast and pancreatic cancers, respectively [20,38]. Our data showed that FTO enhanced the expression of P21/Nrf2 by mediating their mRNA m6A demethylation. Another study found that FTO positively correlated with the up-regulation of P21 in an IL-17A-induced endothelial cell senescence model [22], which further supports our findings. FTO was also found to inhibit oxidative stress by mediating m6A demethylation of Nrf2 [39]. This evidence suggests FTO activates P21/Nrf2 in a P53 dependent or independent manner by mediating m6A demethylation of P53 or P21/Nrf2.

HuR plays an important role in heart function. In the $HuR^{-/-}$ mice, increased left ventricle wall thickness and fibrosis were observed [40]. Consistently, our data also showed that FTO protected against DOX-induced cardiotoxicity by inhibiting ferrotosis, while inhibition of HuR also blocked the antiferroptotic effect of FTO. The regulation of HuR in ferroptosis was also found in the liver fibrosis model [41]. HuR binds m6A-modified transcripts that are important for m6A modification [23,24]. For example, HuR interacts with ALKBH5-mediated unmethylated nascent transcripts of FOXM1, thereby enhancing FOXM1 expression in glioblastoma stem-like cells [42]. Similarly, HuR can assist in the m6A modification of MELLT3 on MALAT1 in gliomas [43]. In this study, HuR expression was significantly increased by FTO and facilitated FTO-mediated m6A demethylation of P53, P21, and Nrf2. In addition, HuR, an mRNA-binding protein, was found to modulate mRNA stability and/or translation including P21 by binding to the AU-rich element (ARE) and stabilising the corresponding transcripts [44]. HuR can also bind with the 3′UTR of P53 mRNA and promote P53 translation [45]. Moreover, HuR promotes Nrf2 mRNA maturation and nuclear export [46]. This suggests that as a non-class m6A reader or mRNA-binding protein, HuR enhances the stability of P53, P21 and Nrf2 transcripts.

Notably, our study and others showed that P53 and P21 expression were decreased by DOX, which was associated with DOX-induced cardiotoxicity [14,15,18]. In contrast, many other studies have shown that P53 and P21 expression are upregulated by DOX and promote cardiomyocyte apoptosis and cardiac dysfunction [47,48]. In this study, we found that P53 and P21 expression were increased in H9C2 and AC16 cells treated with 10 nM DOX for 24h, but decreased in a dose-dependent manner after DOX treatment at 100, 200, and 400 nM (Fig. 8A and B). In line with our data, P53 and P21 were increased in HepG2 cells after DOX treatment at IC10 and decreased after DOX treatment at IC50 [49]. Consistently, we found that P21 was decreased in H9C2 cells after DOX treatment at the IC50 (200 nM). Moreover, the functions of P53 and P21 were associated with the stage of DOX treatment. For example, the inhibition of P53 activity protects against DOX acute cardiotoxicity. In contrast, inhibiting of P53 activity can increase cardiomyocyte apoptosis during the later stages of DOX treatment [51]. While, in P53 deficient ($P53^{-/-}$) mice, low-dose DOX also can cause the decreases in cardiac oxidative metabolism, mitochondrial mass, mitochondrial genomic DNA homeostasis, and left ventricular systolic dysfunction [52]. Similarly, DOX induced an initial up-regulation of P21 followed by a dramatic decline below baseline, which was observed between 16 and 24 h post-treatment [50]. Long-term DOX treatment induces proteasomal degradation of P21, which exacerbates mitochondrial dysfunction and cardiomyocyte apoptosis. Elevated expression of P21 mitigated DOX cardiotoxicity [50].

Our data showed that P21 inhibition in turn inhibited HuR and P53, indicating that P21 also positively up-regulated HuR and P53. In lined with our data, P21 promotes the expression of P53 in cardiomyocytes, suggesting a positive bidirectional feedback loop between P53 and P21 [53]. However, the underlying mechanism remains unclear. Moreover, the HuR inhibitor KH-3 inhibited the expression of FTO in H9C2 cells. Enrichment of FTO was observed in HuR-RIP, indicating that HuR positively increased the expression of FTO. Similarly, HuR was found to enhance the mRNA stability of METTL14 and ALKBH5 by interacting with their mRNAs [54], HuR was also found to regulate METTL14 by binding to its promoter, a transcriptional factor [55]. Moreover, our study and another showed that HuR could bind to its transcript to enhance its expression [56]. Collectively, our data showed a positive feedback loop for FTO/HuR/P53–P21.

5. Conclusion

Our data suggest the FTO ameliorates DOX-induced cardiotoxicity by inhibiting ferroptosis via P21/Nrf2 activation. FTO activates P21/Nrf2 in a P53-dependent or -independent manner by mediating m6A demethylation. HuR is crucial for FTO mediated regulation of ferroptosis and

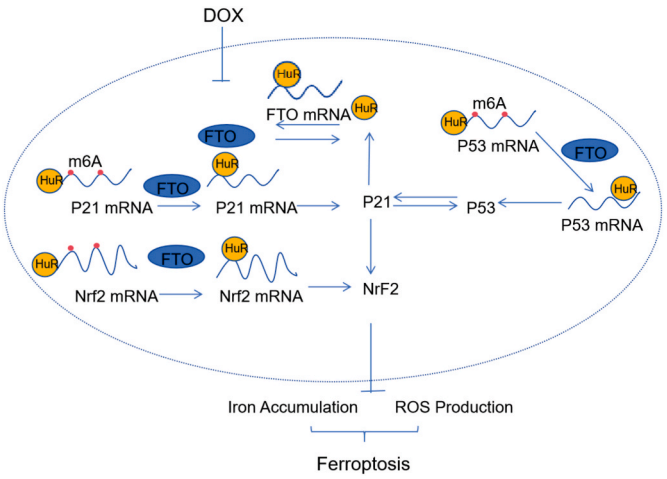

Fig. 9. FTO inhibits DOX-induced ferroptosis by activating P53–P21/Nrf2 in a HuR-dependent m6A manner.Mechanistically, DOX-induced cardiotoxicity was associated with inhibition of FTO. FTO overexpression mediates m6A demethylation of P53, which is up-stream of P21. In addition, FTO also activateS P21/Nrf2 by mediating their mRNA m6A demethylation directly. P21/Nrf2 signaling is important for the anti-ferroptosis effect of FTO. HuR is crucial for FTO-mediated regulations of ferroptosis and P53–P21/Nrf2 by binding with their mRNAs and enhancing their stability. Moreover, P21 in turn, decreased the expression of HuR and P53 and HuR also up-regulated the expression of FTO, suggesting that there is a positive feedback loop for P53–P21.

P53–P21/Nrf2. Moreover, FTO constitutes a positive feedback loop with HuR and P53–P21 (Fig. 9). Our findings provide a novel mechanism underlying the regulation of FTO in DOX-induced cardiotoxicity by inhibiting ferroptosis.

Declarations

All mouse studies were approved by the Institutional Animal Care and Use Committee of Jilin University (2023227).

6. Availability of data and materials

The data that support the findings of this study are available from the corresponding author, upon reasonable request.

CRediT authorship contribution statement

Yunfan Yang: Project administration, Writing – original draft. **Jiajun Ren:** Project administration, Writing – original draft. **Jifeng Zhang:** Methodology, Software. **Henghe Shi:** Formal analysis, Software. **Junnan Wang:** Conceptualization. **Youyou Yan:** Conceptualization, Funding acquisition.

Declaration of competing interest

Our manuscript entitled "**FTO ameliorates doxorubicin-induced cardiotoxicity by inhibiting ferroptosis via P53–P21/Nrf2 activation in a HuR-dependent m6A manner**" complies with the Journal's publication ethics and has not been submitted to any other journals. All authors agreed to the publication of this paper and we have no conflict of interest.

Acknowledgement

This study was supported by Jilin Provincial Natural Science Foundation (20200201601JC).

References

[1] A. Godishala, S. Yang, A. Asnani, Cardioprotection in the modern era of cancer chemotherapy, Cardiol. Rev. 26 (3) (2018) 113–121.
[2] B.P. Lohanathan, B. Rathinasamy, C.Y. Huang, et al., Neferine attenuates doxorubicin-induced fibrosis and hypertrophy in H9c2 cells, J. Biochem. Mol. Toxicol. 36 (7) (2022) e23054.
[3] T. Tadokoro, M. Ikeda, T. Ide, et al., Mitochondria-dependent ferroptosis plays a pivotal role in doxorubicin cardiotoxicity, JCI insight 5 (9) (2020).
[4] X. Fang, H. Wang, D. Han, et al., Ferroptosis as a target for protection against cardiomyopathy, Proc. Natl. Acad. Sci. USA 116 (7) (2019) 2672–2680.
[5] J.P. Friedmann Angeli, M. Schneider, B. Proneth, et al., Inactivation of the ferroptosis regulator Gpx4 triggers acute renal failure in mice, Nat. Cell Biol. 16 (12) (2014) 1180–1191.
[6] M.W. Zhang, X.T. Li, Z.Z. Zhang, et al., Elabela blunts doxorubicin-induced oxidative stress and ferroptosis in rat aortic adventitial fibroblasts by activating the KLF15/GPX4 signaling, Cell stress and chaperones 28 (1) (2023) 91–103.
[7] A. Paramasivam, J. Vijayashree Priyadharsini, S. Raghunandhakumar, N6-adenosine methylation (m6A): a promising new molecular target in hypertension and cardiovascular diseases, Hypertens. Res. 43 (2) (2020) 153–154.
[8] H. Shen, K. Xie, Y. Tian, et al., N6-methyladenosine writer METTL3 accelerates the sepsis-induced myocardial injury by regulating m6A-dependent ferroptosis, Apoptosis (2023) 1–11.
[9] P. Pang, W. Si, H. Wu, et al., YTHDF2 Promotes Cardiac Ferroptosis via Degradation of SLC7A11 in Cardiac Ischemia–Reperfusion Injury[J], Antioxidants & Redox Signaling, 2023.
[10] X. Chen, L. Zhang, Y. He, et al., Regulation of m6A modification on ferroptosis and its potential significance in radiosensitization, Cell Death Discovery 9 (1) (2023) 343.
[11] P. Yu, J. Wang, G. Xu, et al., RNA m6A-Regulated Circ-Znf609 Suppression Ameliorates Doxorubicin-Induced Cardiotoxicity by Upregulating FTO[J], JACC: Basic to Translational Science, 2023.
[12] W.M. Huang, Z.X. Li, Y.H. Wu, et al., m6A demethylase FTO renders radioresistance of nasopharyngeal carcinoma via promoting OTUB1-mediated anti-ferroptosis, Translational Oncology 27 (2023) 101576.
[13] F.H. Ji, X.H. Fu, G.Q. Li, et al., FTO prevents thyroid cancer progression by SLC7A11 m6A methylation in a ferroptosis-dependent manner, Front. Endocrinol. 13 (2022) 857765.
[14] D. Venkatesh, B.R. Stockwell, C. Prives, P21 can be a barrier to ferroptosis independent of P53, Aging (Albany NY) 12 (18) (2020) 17800.
[15] Z. Cheng, L.A. DiMichele, M. Rojas, et al., Focal adhesion kinase antagonizes doxorubicin cardiotoxicity via p21Cip1, Journal of molecular and cellular cardiology 67 (2014) 1–11.
[16] W. Chen, Z. Sun, X.J. Wang, et al., Direct interaction between Nrf2 and p21Cip1/WAF1 upregulates the Nrf2-mediated antioxidant response, Molecular cell 34 (6) (2009) 663–673.
[17] X. Song, D. Long, Nrf2 and ferroptosis: a new research direction for neurodegenerative diseases, Front. Neurosci. 14 (2020) 267.
[18] A. Tarangelo, S. Dixon, The P53-P21 pathway inhibits ferroptosis during metabolic stress, Oncotarget 9 (37) (2018) 24572.
[19] L. Jiang, N. Kon, T. Li, S.J. Wang, T. Su, H. Hibshoosh, et al., Ferroptosis as a P53-mediated activity during tumour suppression, Nature 520 (2015) 57–62.
[20] L. Cheng, X. Zhang, Y.Z. Huang, et al., Metformin exhibits antiproliferation activity in breast cancer via miR-483-3p/METTL3/m6A/P21 pathway, Oncogenesis 10 (1) (2021) 7.
[21] Q. Li, X. Li, H. Tang, et al., NSUN2-mediated m5C methylation and METTL3/METTL14-mediated m6A methylation cooperatively enhance p21 translation, J. Cell. Biochem. 118 (9) (2017) 2587–2598.
[22] N. Li, R. Luo, W. Zhang, et al., IL-17A promotes endothelial cell senescence by up-regulating the expression of FTO through activating JNK signal pathway, Biogerontology 24 (1) (2023) 99–110.
[23] Y.Z. Chang, R.C. Chai, B. Pang, et al., METTL3 enhances the stability of MALAT1 with the assistance of HuR via m6A modification and activates NF-κB to promote the malignant progression of IDH-wildtype glioma, Cancer letters 511 (2021) 36–46.
[24] S.J. Cho, J. Zhang, X. Chen, RNPC1 modulates the RNA-binding activity of, and cooperates with, HuR to regulate p21 mRNA stability, Nucleic acids research 38 (7) (2010) 2256–2267.
[25] R. Dong, K. Polireddy, X. Wu, et al., An RNA binding protein, HuR, in pancreatic cancer EMT, metastasis, and CSC, Faseb. J. 33 (S1) (2019), 674.10-674.10.
[26] J. Zhang, T. Qiu, X. Yao, et al., Insights into the role of N6-methyladenosine in ferroptosis, Biomed. Pharmacother. 165 (2023) 115192.
[27] W.M. Huang, Z.X. Li, Y.H. Wu, et al., m6A demethylase FTO renders radioresistance of nasopharyngeal carcinoma via promoting OTUB1-mediated anti-ferroptosis, Translational Oncology 27 (2023) 101576.
[28] F.H. Ji, X.H. Fu, G.Q. Li, et al., FTO prevents thyroid cancer progression by SLC7A11 m6A methylation in a ferroptosis-dependent manner, Front. Endocrinol. 13 (2022) 857765.
[29] W. Li, G. Huang, J. Wei, et al., ALKBH5 inhibits thyroid cancer progression by promoting ferroptosis through TIAM1–Nrf2/HO-1 axis, Mol. Cell. Biochem. 478 (4) (2023) 729–741.
[30] D. Lv, C. Zhong, D. Dixit, et al., EGFR Promotes ALKBH5 Nuclear Retention to Attenuate N6-Methyladenosine and Protect against Ferroptosis in glioblastoma[J], Molecular Cell, 2023.

[31] H. Li, T. Zou, S. Meng, et al., p21 protects cardiomyocytes against ischemia-reperfusion injury by inhibiting oxidative stress, Mol. Med. Rep. 17 (3) (2018) 4665–4671.
[32] C.D. Venkatakrishnan, K. Dunsmore, H. Wong, et al., HSP27 regulates p53 transcriptional activity in doxorubicin-treated fibroblasts and cardiac H9C2 cells: p21 upregulation and G2/M phase cell cycle arrest, Am. J. Physiol. Heart Circ. Physiol. 294 (4) (2008) H1736–H1744.
[33] Y. Gao, B. Chen, R. Wang, et al., Knockdown of RRM1 in tumor cells promotes radio-/chemotherapy induced ferroptosis by regulating p53 ubiquitination and p21-GPX4 signaling axis, Cell Death Discovery 8 (1) (2022) 343.
[34] X. Hou, J. Shi, L. Sun, et al., The involvement of ERK1/2 and p38 MAPK in the premature senescence of melanocytes induced by H2O2 through a p53-independent p21 pathway, J. Dermatol. Sci. 105 (2) (2022) 88–97.
[35] W. Ke, L. Zhang, X. Zhao, et al., p53 m6A modulation sensitizes hepatocellular carcinoma to apatinib through apoptosis, Apoptosis 27 (5–6) (2022) 426–440.
[36] Y. Wang, W. Zhu, X. Chen, et al., Selenium-binding protein 1 transcriptionally activates p21 expression via p53-independent mechanism and its frequent reduction associates with poor prognosis in bladder cancer, J. Transl. Med. 18 (2020) 1–13.
[37] M.R. Kibbe, J. Li, S. Nie, et al., Inducible nitric oxide synthase (iNOS) expression upregulates p21 and inhibits vascular smooth muscle cell proliferation through p42/44 mitogen-activated protein kinase activation and independent of p53 and cyclic guanosine monophosphate, J. Vasc. Surg. 31 (6) (2000) 1214–1228.
[38] F. Xie, Y. Zheng, W. Fu, et al., The m6A methyltransferase METTL16 inhibits the proliferation of pancreatic adenocarcinoma cancer cells via the p21 signaling pathway, Front. Oncol. 13 (2023) 1138238.
[39] L. Hou, S. Li, S. Li, et al., FTO inhibits oxidative stress by mediating m6A demethylation of Nrf2 to alleviate cerebral ischemia/reperfusion injury, J. Physiol. Biochem. 79 (1) (2023) 133–146.
[40] A.R. Guarnieri, S.R. Anthony, A. Gozdiff, et al., Adipocyte-specific deletion of HuR induces spontaneous cardiac hypertrophy and fibrosis, Am. J. Physiol. Heart Circ. Physiol. 321 (1) (2021) H228–H241.
[41] R. Que, M. Cao, Y. Dai, et al., Decursin ameliorates carbon-tetrachloride-induced liver fibrosis by facilitating ferroptosis of hepatic stellate cells, Biochem. Cell. Biol. 100 (5) (2022) 378–386.
[42] S. Zhang, B.S. Zhao, A. Zhou, et al., m6A demethylase ALKBH5 maintains tumorigenicity of glioblastoma stem-like cells by sustaining FOXM1 expression and cell proliferation program, Cancer Cell 31 (4) (2017) 591–606. e6.
[43] Y.Z. Chang, R.C. Chai, B. Pang, et al., METTL3 enhances the stability of MALAT1 with the assistance of HuR via m6A modification and activates NF-κB to promote the malignant progression of IDH-wildtype glioma, Cancer letters 511 (2021) 36–46.
[44] W. Wang, H. Furneaux, H. Cheng, et al., HuR regulates p21 mRNA stabilization by UV light, Molecular and cellular biology 20 (3) (2000) 760–769.
[45] K. Mazan-Mamczarz, S. Galbán, I.L. de Silanes, et al., RNA-binding protein HuR enhances p53 translation in response to ultraviolet light irradiation, Proc. Natl. Acad. Sci. USA 100 (14) (2003) 8354–8359.
[46] J.R. Poganik, M.J.C. Long, M.T. Disare, et al., Post-transcriptional regulation of Nrf2-mRNA by the mRNA-binding proteins HuR and AUF1, Faseb. J. 33 (12) (2019) 14636.
[47] Y. Shizukuda, S. Matoba, O.Y. Mian, et al., Targeted disruption of p53 attenuates doxorubicin-induced cardiac toxicity in mice[J]. 71, Mol. Cell. Biochem. 273 (2005) 25–32.
[48] J. Terrand, B. Xu, S. Morrissy, et al., p21WAF1/Cip1/Sdi1 knockout mice respond to doxorubicin with reduced cardiotoxicity, Toxicol. Appl. Pharmacol. 257 (1) (2011) 102–110.
[49] T. Lee, T. Lau, I. Ng, Doxorubicin-induced apoptosis and chemosensitivity in hepatoma cell lines, Cancer Chemother. Pharmacol. 49 (2002) 78–86.
[50] Z. Cheng, L.A. DiMichele, M. Rojas, et al., Focal adhesion kinase antagonizes doxorubicin cardiotoxicity via p21Cip1, Journal of molecular and cellular cardiology 67 (2014) 1–11.
[51] W. Zhu, W. Zhang, W. Shou, et al., P53 inhibition exacerbates late-stage anthracycline cardiotoxicity, Cardiovasc. Res. 103 (1) (2014) 81–89.
[52] J. Li, P. Wang, N.A. Long, et al., p53 prevents doxorubicin cardiotoxicity independently of its prototypical tumor suppressor activities, Proc. Natl. Acad. Sci. USA 116 (39) (2019) 19626–19634.
[53] J. Hong, Y.Y. Ding, J.M. Li, et al., Self-limiting bidirectional positive feedback between P53 and P21 is involved in cardiac hypertrophy, Eur. J. Pharmacol. 932 (2022) 175239.
[54] S. Panneerdoss, V.K. Eedunuri, P. Yadav, et al., Cross-talk among writers, readers, and erasers of m6A regulates cancer growth and progression, Sci. Adv. 4 (10) (2018) eaar8263.
[55] H. Wang, W. Wei, Z.Y. Zhang, et al., TCF4 and HuR mediated-METTL14 suppresses dissemination of colorectal cancer via N6-methyladenosine-dependent silencing of ARRDC4, Cell Death Dis. 13 (1) (2021) 3.
[56] W. Dai, G. Zhang, E.V. Makeyev, RNA-binding protein HuR autoregulates its expression by promoting alternative polyadenylation site usage, Nucleic acids research 40 (2) (2012) 787–800.